TU Delft

Delft University of Technology

Document Version
Final published version

Licence
Dutch Copyright Act (Article 25fa)

Citation (APA)
van Peijpe, C., Ghanipoor, F., de Loore, Y., Hacking, P., van de Wouw, N., & Mohajerin Esfahani, P. (2026). Fault Isolation for the Ink Deposition Process in High-End Industrial Printers. *IEEE Transactions on Control Systems Technology*, *34*(3), 1617-1624. https://doi.org/10.1109/TCST.2026.3664927

Important note
To cite this publication, please use the final published version (if applicable).
Please check the document version above.

Copyright
In case the licence states “Dutch Copyright Act (Article 25fa)”, this publication was made available Green Open Access via the TU Delft Institutional Repository pursuant to Dutch Copyright Act (Article 25fa, the Taverne amendment). This provision does not affect copyright ownership.
Unless copyright is transferred by contract or statute, it remains with the copyright holder.

Sharing and reuse
Other than for strictly personal use, it is not permitted to download, forward or distribute the text or part of it, without the consent of the author(s) and/or copyright holder(s), unless the work is under an open content license such as Creative Commons.

Takedown policy
Please contact us and provide details if you believe this document breaches copyrights.
We will remove access to the work immediately and investigate your claim.

*This work is downloaded from Delft University of Technology.*

# Fault Isolation for the Ink Deposition Process in High-End Industrial Printers

Casper van Peijpe, Farhad Ghanipoor, Youri de Loore, Pim Hacking, Nathan van de Wouw, *Fellow, IEEE*, and Peyman Mohajerin Esfahani

***Abstract*—This brief presents a mathematical framework for modeling the dynamic effects of three fault categories and six fault variants in the ink channels of high-end industrial printers. It also introduces a hybrid approach that combines model-based and data-based methods to detect and isolate these faults effectively. A key challenge in these systems is that the same piezo device is used for actuation (generating ink droplets) and for sensing, and, as a consequence, sensing is only available when there is no actuation. The proposed fault detection (FD) filter, based on the healthy model, uses the piezo self-sensing signal to generate a residual, while taking the above challenge into account. The system is flagged as faulty if the residual energy exceeds a threshold. Fault isolation (FI) is achieved through linear regression (LR) or a k-nearest neighbors (KNN) approach to identify the most likely fault category and variant. The resulting hybrid fault detection and isolation (FDI) method overcomes traditional limitations of model-based methods by isolating different types of faults affecting the same entries (i.e., equations) in the ink channel dynamics. Moreover, it is shown to outperform purely data-driven methods in FI, especially when data is scarce. Experimental validation demonstrates superior FDI performance compared to state-of-the-art methods.**

***Index Terms*—Fault detection (FD), fault diagnosis, industrial printing, ink channel dynamics, k-nearest neighbors (KNN) algorithm (KNN), linear regression (LR), machine learning.**

## I. Introduction

OVER the past decades, fault diagnosis has been a focal point of research because of its vital role in maintaining the safety and reliability of engineering systems [1], [2]. In this brief, the systems of interest are the printers of Canon Production Printing (CPP). CPP is a Canon subsidiary located in Venlo, the Netherlands, that develops, manufactures, and sells high-end industrial printers [3]. Accurate fault diagnosis for the ink channels of these printers is essential for improving print quality and maintenance services. The ink channels are subject to different faults, such as empty channels, partial or complete nozzle blockage, or drying of local ink [4], [5]. All of these faults degrade the image and printing quality.

Preventing low-quality prints has several advantages: increasing customer satisfaction, reducing costly reprints, and minimizing environmental impact. Therefore, it is beneficial to detect and isolate faults early so compensation can be applied before print quality is reduced.

The printers considered in this brief consist of various components that work together to ensure proper functioning. The focus is on the ink channels, of which hundreds to thousands are located in the printheads, depending on the printer. In Fig. 1, a decomposition is shown indicating where each component is located and how many are inside the component to its left. See [6] and [7] for more details about the printers and printheads.

Detecting and isolating faults in the ink channel is challenging. Both the time scale and the dimension of the system are microscopic, with a typical piezo self-sensing signal being tens of microseconds long [5], an actuation chamber a few millimeters long, and drop ejection nozzles just tens of micrometers in diameter [4]. These small scales result in tiny physical quantities, making system states difficult to observe. A piezo self-sensing signal can be obtained by using the piezo actuator (used to induce ink deposition) as a sensor, but only after actuation occurs [8], [9], [10]. Furthermore, these printers can collect signals from more than 100 000 ink channels in less than 100 ms [3]. Handling such large data volumes emphasizes the need for computational efficiency. As actuation and sensing cannot occur simultaneously, input–output data is not available at the same time. The state, therefore, cannot be assumed to be zero at the start of sensing, although this assumption is common in the fault diagnosis literature [11], [12], [13].

The frequency content of the self-sensing signals generated by the piezo actuator can be used for fault detection and isolation (FDI) through signal-based fault tree methods with tunable thresholds, which is currently being used by the manufacturer for the health monitoring of their printers. This state-of-practice (SoP) approach can be seen as a data-based method [14], [15], which has the drawback of not directly taking into account any physics-based model of the system (ink channel dynamics). Besides, the thresholds used are manual margins based on experience, making the method nonsystematic and hard to generalize to different printer types.

Motivated by the aforementioned challenges, a hybrid model- and data-based FDI approach is proposed to detect and isolate faults using piezo self-sensing signals. This approach consists of two stages: fault detection (FD), which is the model-based part of the proposed methodology, and fault isolation (FI), which is the data-based part. The proposed method for FD builds upon previous results [11], [12], where the task of FD involves generating a diagnostic signal sensitive

Received 13 November 2025; accepted 20 January 2026. Date of publication 25 March 2026; date of current version 5 May 2026. This work was supported in part by the Digital Twin Project 4.3 (P18-03) within the Perspectief Program through Dutch Research Council (NWO). The work of Peyman Mohajerin Esfahani was supported by European Research Council (ERC) under Grant TRUST-949796. Recommended by Associate Editor J. Mohammadpour Velni. *(Casper van Peijpe and Farhad Ghanipoor contributed equally to this work.) (Corresponding author: Farhad Ghanipour.)*

Casper van Peijpe is with the Delft Center for Systems and Control, Delft University of Technology, 2628 CN Delft, Netherlands (e-mail: C.D.vanPeijpe@tudelft.nl).

Farhad Ghanipour and Nathan van de Wouw are with the Department of Mechanical Engineering, Eindhoven University of Technology, 5612 AZ Eindhoven, Netherlands (e-mail: F.Ghanipoor@tue.nl; N.v.d.Wouw@tue.nl).

Youri de Loore and Pim Hacking are with the Canon Production Printing, 5914 HH Venlo, Netherlands (e-mail: Youri.deLoore@cpp.canon; Pim.Hacking@cpp.canon).

Peyman Mohajerin Esfahani is with the Mechanical and Industrial Engineering, University of Toronto, Toronto, ON M5S1A1, Canada (e-mail: P.MohajerinEsfahani@utoronto.ca).

Digital Object Identifier 10.1109/TCST.2026.3664927

1063-6536 © 2026 IEEE. All rights reserved, including rights for text and data mining, and training of artificial intelligence and similar technologies. Personal use is permitted, but republication/redistribution requires IEEE permission.
See https://www.ieee.org/publications/rights/index.html for more information.

Authorized licensed use limited to: TU Delft Library. Downloaded on May 26,2026 at 12:11:59 UTC from IEEE Xplore. Restrictions apply.

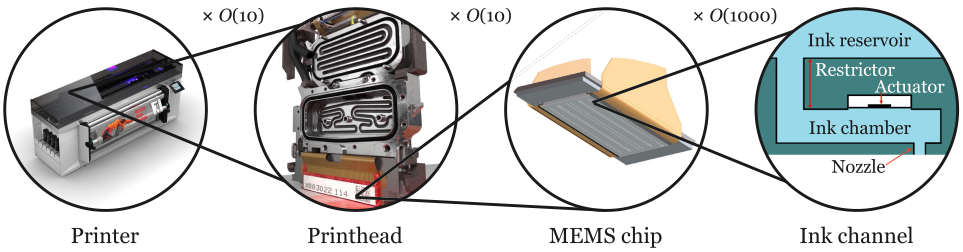



Fig. 1. Decomposition of the printer where each component shown is smaller than and inside of the component to its left.

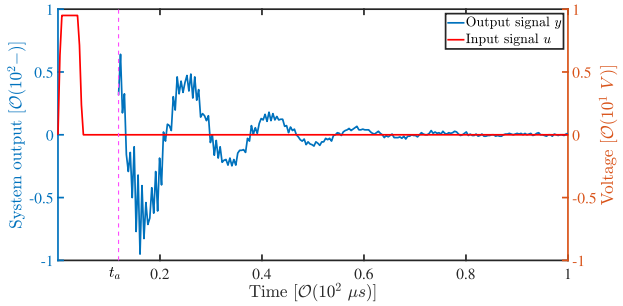



Fig. 2. Typical input (actuation) signal and corresponding output (sensing) signal, with the output starting after the completion of the input at time $t_a$.

to the occurrence of faults, known as the residual. This task is accomplished by designing a model-based filter fed by the piezo self-sensing signal. The filter formulation is modified to account for the system actuation and sensing data not being available simultaneously. For FI, inspired by van der Ploeg et al. [16], an isolation filter is designed using a regression operator, as well as a classification algorithm, both using the output of the FD filter (i.e., residual signal). Contrary to the previous work, (simulated) faulty data is assumed to be available. Additionally, the FI filter design is adjusted to ensure that it can appropriately deal with scenarios in which only one fault can be present at a time (as is the case for the industrial printing use case in this brief).

The main contributions of this brief are as follows.

1) *Modeling printer (ink channel) dynamics and possible faults:* We model the dynamics of ink channels for a class of industrial printers considering the fault categories of: 1) an empty ink channel; 2) a blocked nozzle; and 3) a dried nozzle. The modeling framework includes six different variants of these fault categories that are encountered in practice.
2) *Methodologies for FDI:* In light of the practical limitation of actuation and sensor data being unavailable simultaneously, we develop a tailored FDI filter based on the model, in combination with available labeled experimental data. Moreover, the developed hybrid model-data fault diagnosis method addresses the limitation of conventional model-based approaches by isolating different types of faults that affect the same entries in the ink channel dynamics [13], [17], [18]. This capability is enabled by integrating data-driven classifiers, which effectively distinguish between different patterns in the residual generated by the model-based fault detector filter. Additionally, it is shown that the method outperforms purely data-driven approaches in FI.
3) *Experimental validation on an industrial printer* [3]: The results are validated experimentally, indicating that the proposed method provides superior performance for both FD and FI compared to the current state-of-the-art method.

The content of the remainder of brief is as follows. The problem statement of the printing use case is described in Section II. A solution approach to the problem of FDI is outlined in Section III. The results of this approach with simulated and experimental data are shown in Section IV. Lastly, the conclusions that can be drawn from the results are presented, together with recommendations for future work in Section V.

## II. Printer Dynamics, Faults, and the Diagnosis Problem

The ink channel dynamics of the printer are presented in Section II-A, the possible operational faults are explained in Section II-B, and the problem of FDI is described in Section II-C.

### A. Mathematical Model for Ink Channel Dynamics

The smallest component in Fig. 1, the ink channel, is the subject of this study. When printing, a piezo-electric actuator is (dis)charged, inducing a mechanical deformation which displaces the ink from the ink chamber to both the restrictor and nozzle; see the subfigure on the right side of Fig. 1. A strong enough actuation will lead to a droplet being jetted from the nozzle onto the brief [19]. The movement of the ink is captured in a 4-D state vector, denoted by $x$, which contains the volumes and flow rates displaced through the restrictor and the nozzle when actuating. The single variable voltage discharging the actuator is captured by the input $u$.

The linear differential equations describing the fluid dynamics principles in [5], complemented by the addition of resistance in [4], are used to describe the ink channel dynamics in the healthy case as follows:

$$\underbrace{\begin{bmatrix}\dot{V}_r\\ \dot{V}_n\\ \ddot{V}_r\\ \ddot{V}_n\end{bmatrix}}_{\dot{x}} = \underbrace{\begin{bmatrix}0 & 0 & 1 & 0\\ 0 & 0 & 0 & 1\\ -\frac{1}{I_r\beta_t} & -\frac{1}{I_r\beta_t} & -\frac{R_r}{I_r} & 0\\ -\frac{1}{I_n\beta_t} & -\frac{1}{I_n\beta_t} & 0 & -\frac{R_n}{I_n}\end{bmatrix}}_{A}\underbrace{\begin{bmatrix}V_r\\ V_n\\ \dot{V}_r\\ \dot{V}_n\end{bmatrix}}_{x} + \underbrace{\begin{bmatrix}0\\ 0\\ \frac{b}{I_r\beta_t}\\ \frac{b}{I_n\beta_t}\end{bmatrix}}_{B_u} u, \quad y = \underbrace{\begin{bmatrix}0 & 0 & c & c\end{bmatrix}}_{C}\underbrace{\begin{bmatrix}V_r\\ V_n\\ \dot{V}_r\\ \dot{V}_n\end{bmatrix}}_{x} \tag{1}$$

Authorized licensed use limited to: TU Delft Library. Downloaded on May 26,2026 at 12:11:59 UTC from IEEE Xplore. Restrictions apply.

where $V_r$ and $V_n$, respectively, are the volumes of ink displaced through the restrictor and the nozzle when actuating. The physical parameters $I_r$ and $I_n$ are the inertances in the restrictor and the nozzle, respectively, $R_r$ and $R_n$ are the resistances in the restrictor and the nozzle, respectively, and the constant $\beta_t$ is the total compliance of the system. The input signal $u$ is the voltage applied to the actuator. Actuator constant $b$ captures the relation between the voltage input and the influence on the channel pressure, which contributes proportionally to the time-derivative of the flow rate in the restrictor and nozzle via the factors $b/(I_r\beta_t)$ and $b/(I_n\beta_t)$, respectively. The acquisition constant $c$ captures the relationship between the flow rates (of ink displaced through the restrictor and the nozzle) in the ink chamber and the output signal $y$. Note that a few microseconds after each actuation, the piezoelectric actuator can be used as a sensor to measure $y$ in (1). For a more detailed explanation of the model parameters, see [5]. A typical example of the process trajectories of both actuation and sensor acquisition is plotted in Fig. 2.

Since the actuator acts as a sensor after actuation, the system is treated as autonomous with the nonzero state $x_a(t_a)$ (called the acquisition state) at starting time $t_a$ of the acquisition. As a result, the term related to $B_u$ can be neglected in (1) after $t = t_a$.

### B. Operational Faults

The operational faults studied in this article are caused by changes in some parameters of our mathematical model in (1). These faults are naturally of a multiplicative nature with the internal states of the system $x$. With this in mind, we can model each fault effect on the printer dynamics as follows:

$$\begin{cases} \dot{x}(t) = \left(A + B_{f_i} f_i\right) x(t), \quad i \in \{1, 2, \ldots, n_f\} \\ y(t) = Cx(t) \end{cases} \qquad \text{ODE}(i)$$

where the system matrices $A$ and $C$ are as defined in (1) and the signal $f_i \in \mathbb{R}_+$ is the $i$th fault signal taking values "0" whenever the system is healthy (i.e., no faults) or nonzero values when the fault occurs. Herein, $n_f$ denotes the number of fault variants, which are listed below, and equals six. It is practically reasonable to assume that at most one $i$th fault occurs at a time. Consequently, (ODE($i$)) captures the dynamics representing this sole $i$th fault scenario. For every fault, the matrix term $B_{f_i} f_i$ is added to $A$, where $B_{f_i}$ captures the changes in the parameters of $A$. The matrix $B_{f_i}$ may be different for every fault scenario and contains parameter changes related to that fault. Therefore, matrix $B_{f_i}$ is different for every fault $i$ and generally can be described as follows:

$$B_{f_i} = \begin{bmatrix} 0 & 0 & 0 & 0 \\ 0 & 0 & 0 & 0 \\ \delta\left(\frac{1}{I_r\beta_t}\right)_i & \delta\left(\frac{1}{I_r\beta_t}\right)_i & \delta\left(\frac{R_r}{I_r}\right)_i & 0 \\ \delta\left(\frac{1}{I_n\beta_t}\right)_i & \delta\left(\frac{1}{I_n\beta_t}\right)_i & 0 & \delta\left(\frac{R_n}{I_n}\right)_i \end{bmatrix}.$$

Note that faults that cause a possible change in model structure, potentially leading to a nonlinear model, are not taken into account, and that the studied fault scenarios can be described by a change in $B_{f_i}$. Furthermore, note that in practice, since we do not know the actual entries in the matrix $B_{f_i}$, we model it as matrices with zero and nonzero elements to indicate which equations are affected. These are provided below, along with the fault scenarios.

1) *Empty ink channel (EC):* Refers to a fault in which an ink channel is not filled with ink. An ink channel may be empty before filling or emptied during printing. An empty channel can be modeled as a decrease in inertance of both the restrictor and nozzle, $I_r$ and $I_n$, causing the sensing signal $y$ to oscillate at a higher frequency. The corresponding fault matrix is denoted as $B_{f_1}$, and all nonzero elements in the general fault matrix $B_{f_i}$ are nonzero in $B_{f_1}$ as well.
2) *Blocked nozzle (BN):* Refers to a fault in which a dirt particle is present at the outlet of the nozzle. This causes the nozzle inertance, $I_n$, and resistance, $R_n$, to increase, resulting in a faster decay of the sensing signal $y$. Two different types of blocked nozzle (BN) can be distinguished: 1) *fully blocked nozzle (FBN):* refers to a fault in which a nozzle is fully blocked, implying no printing can be done; and 2) *partially blocked nozzle (PBN):* refers to a fault in which a part of the nozzle is blocked, implying ink exits the nozzle incorrectly. The corresponding fault matrices are denoted as $B_{f_2}$ and $B_{f_3}$, for the FBN and PBN, respectively. Both matrices have the same nonzero elements, which are $B_{f_2}(4,1)$, $B_{f_2}(4,2)$, $B_{f_2}(4,4)$, and similarly $B_{f_3}(4,1)$, $B_{f_3}(4,2)$, $B_{f_3}(4,4)$.
3) *Dried nozzle (DN):* Refers to a fault in which the ink at the nozzle's outlet has evaporated. This causes the viscosity to increase and therefore the resistance $R_n$ to locally increase, leading to a faster decay of the sensing signal $y$. Three different drying levels are distinguished: 1) slightly dried nozzle (SDN); 2) intermediately dried nozzle (IDN); and 3) deeply dried nozzle (DDN). The corresponding fault matrices are denoted as $B_{f_4}$, $B_{f_5}$, and $B_{f_6}$, for the SDN, IDN, and DDN, respectively. All three matrices have the same nonzero element, which is $B_{f_4}(4,4)$ and similarly $B_{f_5}(4,4)$ and $B_{f_6}(4,4)$.

Simultaneous faults are excluded from the scope of this work, given that their probability of occurrence is about $10^6$ times lower than that of single faults, and thus their impact is considered negligible for practical purposes. The problem to be solved in this brief can now be stated.

### C. Fault Detection and Isolation Problem

We aim to design an FD filter that can distinguish between healthy and faulty systems using the output data $y(t)$ and an approximated acquisition state $\hat{x}_a$. The FD filter generates a residual signal $r$ that indicates whether the measurements are healthy or are affected by the fault signal $f_i$. Formally, the residual can be represented as a function $r(x_a, f_i)$, and the FD design is ideally defined by the following mapping requirements:

$$x_a \mapsto r(x_a, 0) \equiv 0 \tag{2a}$$

$$f_i \mapsto r(x_a, f_i) \neq 0 \quad \forall i \in \{1, 2, \ldots, n_f\}. \tag{2b}$$

Authorized licensed use limited to: TU Delft Library. Downloaded on May 26,2026 at 12:11:59 UTC from IEEE Xplore. Restrictions apply.

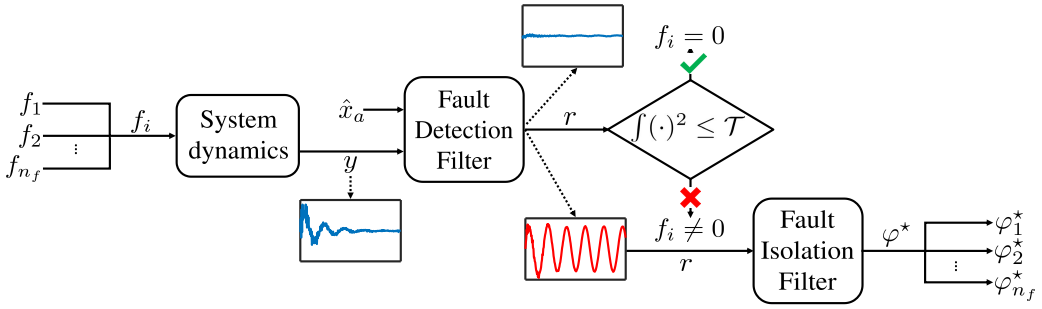



Fig. 3. Overview of the proposed FDI scheme.

For FI, conventional model-based methods, such as [11], use filter banks, with each filter sensitive to one fault and insensitive to others. This approach fails when faults affect the same system dynamics entries. To address this challenge, we aim to design an FI filter capable of isolating the occurring fault using the output of the FD filter, $r$, building on the results in [16]. The FI filter is trained offline using available labeled experimental data for each fault scenario. In the online implementation, the filter generates a vector $\varphi^\star$ (see the output of right block in Fig. 3), where each row represents the percentage of occurrence for each fault scenario, and the fault with the highest percentage is considered to be the occurring fault.

## III. Fault Detection and Isolation Approach

In this section, the proposed solution is presented. Fig. 3 illustrates an overview of the proposed FDI scheme, where different types of faults $f_i$ entering the system are detected and isolated. The methods for FD and FI are provided in Sections III-A and III-B, respectively.

### A. FD Filter

As a preliminary step, an accurate model is obtained using an off-the-shelf gray-box system identification method in MATLAB, namely extended least squares for parameter estimation [20]. This method uses healthy sensor data to estimate system parameters in (1) via solving the following optimization problem:

$$\{A, C, \hat{x}_a\} = \underset{A,C,\hat{x}_a}{\arg\min} \int_{t_a}^{t_f} \left| y(t) - Ce^{At}\hat{x}_a \right| dt \tag{3}$$

where $t_f$ denotes the final time of the signal $y$ collected from the printer. The optimization problem is solved using the interior-point algorithm [21, Ch. 11] and yields an MSE of $2.48 \times 10^{-18}$. The resulting matrices $A$ and $C$ and the estimated acquisition state $\hat{x}_a$ are then used to develop a model-based FD filter.

To construct the FD filter, first, the state-space representation of the system in (ODE($i$)) is converted from the time domain to the Laplace domain as follows:

$$\begin{cases} sX(s) - x_a = AX(s) + B_{f_i}\Psi_i(s) \\ Y(s) = CX(s) \end{cases} \tag{4}$$

where $s \in \mathbb{C}$ is the complex Laplace variable used in the Laplace transform. $X(s), Y(s)$, and $\Psi_i(s)$ are the Laplace transforms of $x(t), y(t)$, and $f_i x(t)$, respectively. Equation (4) can be written as follows:

$$\underbrace{\begin{bmatrix} -sI + A \\ C \end{bmatrix}}_{H(s)=H_0+H_1 s} X(s) + \begin{bmatrix} x_a \\ 0 \end{bmatrix} + \underbrace{\begin{bmatrix} 0 \\ -I \end{bmatrix}}_{L(s)} Y(s) + \underbrace{\begin{bmatrix} B_{f_i} \\ 0 \end{bmatrix}}_{F_i(s)} \Psi_i(s) = 0 \qquad \text{DAE}(i)$$

where $H(s) \in \mathbb{C}^{(n+m)\times n}$, $L(s) \in \mathbb{C}^{(n+m)\times m}$, and $F_i(s) \in \mathbb{C}^{(n+m)\times n}$, for all $i \in \{1, 2, \ldots, n_f\}$. This system representation is also known as the differential-algebraic equation (DAE) (represented in the Laplace domain).

The FD filter can be stated as follows, generating the residual signal defined in the Laplace domain:

$$R(s) := \frac{N(s)L(s)}{\alpha(s)} Y(s) + \frac{N(s)}{\alpha(s)} \begin{bmatrix} \hat{x}_a \\ 0 \end{bmatrix} \tag{5}$$

where $R \in \mathbb{C}$ is the residual in the Laplace domain, $\hat{x}_a$ denotes the approximated acquisition state from (3), $N(s)$ is designed to solve the problem stated in Section II-C [or more specifically to satisfy (2)], and $\alpha(s)$ is chosen such that the transfer function of the residual generator $R(s)$ is (strictly) proper. The method used to design $\alpha(s)$ is described later. This residual can be transformed to the time domain to form the signal $r$. To design $N(s)$, the residual in (5) must be expressed in terms of both state-dependent and fault-dependent terms. It follows from (5) and (DAE($i$)) that

$$R(s) = -\frac{N(s)H(s)}{\alpha(s)} X(s) - \frac{N(s)F_i(s)}{\alpha(s)} \Psi_i(s) + \frac{N(s)}{\alpha(s)} \begin{bmatrix} \hat{x}_a - x_a \\ 0 \end{bmatrix}. \tag{6}$$

To satisfy (2a), the first term in (6) must be zero (i.e., $N(s)H(s) = 0$). Similarly, to satisfy (2b), the second term must be nonzero (i.e., $N(s)F_i(s) \neq 0$). It is shown in [11] that these conditions on the transfer functions can be expressed in terms of matrices as follows:

$$\bar{N}\bar{H} = 0 \tag{7a}$$

$$\bar{N}\bar{F}_i \neq 0 \quad \forall i \in \{1, 2, \ldots, n_f\} \tag{7b}$$

with $\bar{H} \in \mathbb{R}^{d_N(n+m)\times n(d_N+1)}$ as

$$\bar{H} := \begin{bmatrix} H_0 & H_1 & & \\ & \ddots & \ddots & \\ & & H_0 & H_1 \end{bmatrix} \Big\} d_N$$

Authorized licensed use limited to: TU Delft Library. Downloaded on May 26,2026 at 12:11:59 UTC from IEEE Xplore. Restrictions apply.

where $H_0$ and $H_1$ as defined in (DAE($i$)), $d_N$ is the order of the filter, $\bar{N} \in \mathbb{R}^{1\times d_N(n+m)}$, and $\bar{F}_i \in \mathbb{R}^{d_N(n+m)\times nd_N}$ as given by the following equation:

$$\bar{F}_i := \left.\begin{bmatrix} F_i & & \\ & \ddots & \\ & & F_i \end{bmatrix}\right\} d_N$$

where $F_i$ as defined in (DAE($i$)). Generally, to create the FD filter, the linear programming problem in (7) is solved [11]. However, for this specific system (i.e., the ink channel system), the linear programming constraint (7a) has only one solution, meaning solving the linear programming problem is not needed. An approach to design $\bar{N}$ is to calculate the left null space of $\bar{H}$ as $\bar{N} = (\mathcal{N}(\bar{H}^\top))^\top = \begin{bmatrix} N_0 & N_1 & \cdots & N_{d_N} \end{bmatrix}$.

As for implementation purposes, the FD filter formulation should be derived in the Laplace domain, $\bar{N}$ can be converted to $N(s)$ using

$$N(s) := \sum_{i=0}^{d_N} N_i s^i.$$

Note that clearly from (6), it can been verified that if $\hat{x}_a - x_a$ is small, the residual signal will only generate the second term, which is zero in the healthy case because $\Psi_i(s)$ (i.e., the Laplace transform of $f_i x(t)$) is zero, and nonzero when a fault occurs, as the condition in (7b) imposes.

Due to errors caused by approximation of the acquisition state (i.e., $\hat{x}_a - x_a$), modeling uncertainties, and measurement noise, a nonzero residual does not necessarily indicate that the system is faulty, which can lead to some healthy cases being misidentified as faulty. Therefore, to determine whether a residual signal is faulty, a threshold $\mathcal{T}$ on the energy of the residual signal, defined as the integral of the square of the signal, is established as follows:

$$\mathcal{T} = \mu \max_{r_h \in \mathcal{S}_h} \left( \int_{t_a}^{t_f} r_h^2(t)\, dt \right) \tag{8}$$

where $\mathcal{S}_h$ is the healthy residual dataset which is produced by passing measurements $y$, including measurement noise, through the FD filter, $r_h$ represents the healthy residuals taken from this dataset, and $\mu \in \mathbb{R}_+$ is a user-determined factor designed to make the detection method more robust against false alarms caused by approximation errors, modeling uncertainties, and measurement noise (see Section IV-B for design examples). The selection of $\mu$ can be performed using the receiver operating characteristic (ROC) curve, which represents the tradeoff between true positive and false positive rates across different threshold settings [22]. If the threshold is exceeded by the residual energy (i.e., $\int_{t_a}^{t_f} r^2(t)dt$), the system is classified as faulty (see Fig. 3). Besides this threshold, other metrics, such as the maximum value of the residual, which may be computationally faster, can also be used to determine whether a signal is faulty.

The poles of the filter, represented by the denominator $\alpha(s)$ in (5), need to be selected carefully. In [11], the denominator of the FD filter is chosen as an arbitrary transfer function of sufficiently high order, with roots having negative real parts to ensure the transfer function of the filter is both proper and stable. However, it has been observed that the denominator can influence the performance of the filter for the system under consideration.

In this brief, since the energy of the residual is used for FD, the FD filter denominator is designed to amplify the energy of the residual, making faults easier to detect. This is achieved by placing two marginally stable poles of the FD filter at $s = \pm\omega_r i$, where $\omega_r$ is the desired residual frequency, which can be chosen arbitrarily. The frequency can be selected so that a desired number of oscillations occurs within a known time frame $T$. Since this pole pair does not have a negative real part, the residual does not converge to zero, and the energy continues to increase, making the fault more apparent than when the energy stagnates over time, which is the case when using stable poles. This amplifies the presence of a fault, as a faulty residual results in a larger amplitude compared to a healthy residual. The remaining poles are chosen to be asymptotically stable, and can be chosen such that they partially filter out high-frequency noise. Thus, the denominator can be expressed as follows:

$$\alpha(s) = \left(s^2 + \omega_r^2\right)\beta(s), \quad \omega_r = \frac{n_o}{T}$$

where $\beta(s)$ is a transfer function with roots with negative real parts of order $d_N - 2$, and $n_o$ is the desired number of oscillations.

Once a fault has been detected, the next step is to isolate the detected fault. Toward this goal, an FI filter is designed in what follows.

### B. FI Filter

The FI filter is inspired by van der Ploeg et al. [16], where a linear regression (LR) model is also used for FI. This approach assumes prior availability of labeled faulty data and a model that accounts for specific fault scenarios in order to train the FI filter, which limits its applicability to technical systems where such data and models are accessible, such as the printer system studied here. The LR models are trained offline in a discrete setting. Therefore, for offline training, continuous residuals obtained from the proposed FD filter should be discretized, and the $N$ discretized residuals per fault class are averaged for each fault scenario as follows:

$$\rho_i[k] = \frac{1}{N}\sum_{j=1}^{N} r_i^j[k] \quad \forall i \in \{1, 2, \ldots, n_f\},\ k \in \{k_a, \ldots, k_f\}$$

where $\rho_i[k] \in \mathbb{R}$ represents the average residual for each fault class $i$ (see the offline training part in Fig. 4, where only three faults are shown for simplicity), and $k_a, k_f$ are the samples corresponding to $t_a, t_f$, respectively. Next, the matrix $R$, containing the averaged residuals for each fault class $\rho_i[k]$, can be constructed as follows:

$$R = \begin{bmatrix} \rho_1[k_a] & \rho_2[k_a] & \cdots & \rho_{n_f}[k_a] \\ \rho_1[k_a+1] & \rho_2[k_a+1] & \cdots & \rho_{n_f}[k_a+1] \\ \vdots & \vdots & \ddots & \vdots \\ \rho_1[k_f] & \rho_2[k_f] & \cdots & \rho_{n_f}[k_f] \end{bmatrix}.$$

During the online isolation process, LR is used to identify which expected residual $\rho_i[k]$, obtained from offline training,

Authorized licensed use limited to: TU Delft Library. Downloaded on May 26,2026 at 12:11:59 UTC from IEEE Xplore. Restrictions apply.

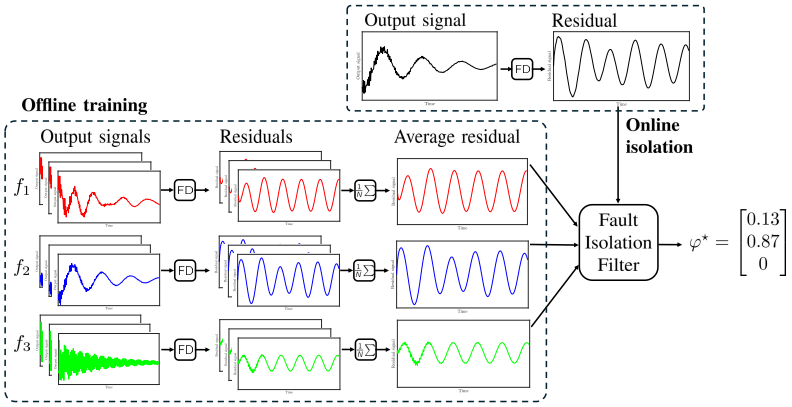



Fig. 4. Schematic overview of the offline training (design) and online application of the FI filter.

is closest to the measured residual signal $r$ to be isolated (see the online isolation part in Fig. 4). The LR model quantifies the contribution of each fault as a vector $\varphi^\star \in \mathbb{R}_+^{n_f}$, which is the solution to the following optimization problem:

$$\varphi^\star = \begin{cases} \arg\min\limits_{\varphi} & \|R\varphi - r\| \\ \text{s.t.} & \sum_{i=1}^{n_f} \varphi_i = 1 \\ & \varphi_i \geq 0, \quad \forall i \in \{1, 2, \ldots, n_f\} \end{cases}$$

where

$$(\varphi)^\top = \begin{bmatrix} \varphi_1 & \ldots & \varphi_{n_f} \end{bmatrix}$$

is used as a regressor. The fault index $i^\star$ corresponding to the highest value in $\varphi^\star$ is considered as the isolated fault, i.e., $i^\star = \arg\max_i \varphi_i^\star, i \in \{1, 2, \ldots, n_f\}$ (for the simplified example illustrated in Fig. 4, $i^\star$ is 2). Instead of LR models, other classifiers, such as the k-nearest neighbors (KNN) algorithm, can be used (see [23]). In this case, the residual signal is assigned to the class of its nearest neighbor.

In the following sections, the FD and FI filters are evaluated using both simulation and experimental data concerning the ink channel dynamics in an industrial printer.

## IV. Simulation and Experimental Results

First, the structure of the data is analyzed in Section IV-A. Then the FD and FI filters are tested for both the simulation and experimental data in Sections IV-B and IV-C, respectively.

### A. Data Analysis

To evaluate both filters, simulated data and experimental data are used. Simulated data is generated based on knowledge of faults and the nature of the available experimental data. 3825 output signals, $y$, are generated, where 2475 are healthy signals, and every fault class contains 225 signals. Hence, all of the six fault classes mentioned in Section II are considered. One healthy example and three examples of faulty signals per fault category are illustrated in Fig. 5.

Experimental data is collected by purposely drying the nozzle. The procedure to overcome a drying nozzle, called prefiring (mixing the ink in the nozzle and ink chamber to bring the ink in the nozzles back to a usable viscosity), is performed to collect data for fault scenarios ranging from deeply dried to healthy. Three datasets are generated: the first, with 48 signals, represents healthy nozzles, where sufficient prefires remove all dried ink. The second, with 39 signals, represents IDNs, where some prefires partially remove dried ink. The third, with 60 signals, represents DDNs, with no prefires performed. Two examples of measured faulty signals per fault category are illustrated in Fig. 6. Notably, separate datasets of the same length as the test data are used for the offline training of the FI filter for both the simulated and experimental data.

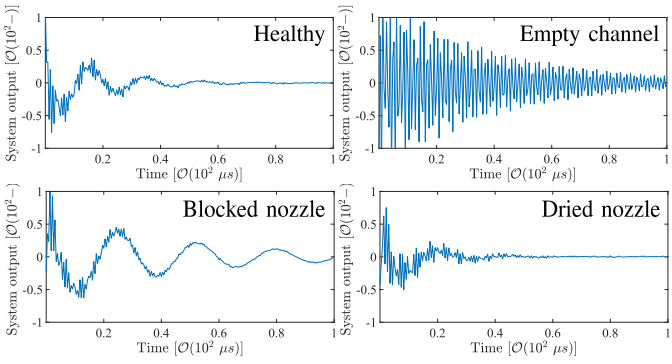



Fig. 5. Examples of sensing signals $y$ for simulated fault categories (here $t_a = 0$).

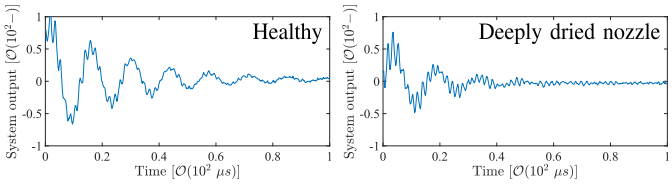



Fig. 6. Examples of sensing signals $y$ for experimental fault categories (here $t_a = 0$).

### B. FD Results

The preliminary system identification results, obtained using the off-the-shelf gray-box method in MATLAB (explained in Section III-A), are provided in the Appendix. The values for $\mu$ in (8) were determined by maximizing the Total Detection Rate (TDR) [24] while keeping the false alarm rate (FAR) [24] as close to zero as possible for different values of $\mu$. The

Authorized licensed use limited to: TU Delft Library. Downloaded on May 26,2026 at 12:11:59 UTC from IEEE Xplore. Restrictions apply.

TABLE I

FD FILTER RESULTS FOR THE SIMULATED DATA

| | | FD filter | |
|---|---|---|---|
| | | Healthy | Faulty |
| Ground truth | Healthy | 2474 | 1 |
| | Faulty | 92 | 1258 |

TABLE II

FD FILTER RESULTS FOR THE EXPERIMENTAL DATA

| | | FD filter | |
|---|---|---|---|
| | | Healthy | Faulty |
| Ground truth | Healthy | 48 | 0 |
| | Faulty | 0 | 99 |

values are $\mu = 1$ and $\mu = 2$ for simulated and experimental data, respectively.

We present the FD results of the proposed method by comparing it with the SoP approach. The SoP method relies on a signal-based fault tree approach with tunable thresholds, which are adjusted based on experience. For further details on the SoP method, refer to [14], [15].

The FD results of the simulated data are summarized in Table I. The proposed FD filter achieves a TDR of 97.6%, surpassing the 93.9% of the manufacturer's current method. Its FAR is 0.04%, compared to 0% for the SoP approach. The substantial improvement in fault detectability halves the number of false detections, underscoring the superior reliability of the proposed approach compared to the SoP method. Furthermore, the computational complexity is lowered from the SoP's $\mathcal{O}(n \log n)$ to $\mathcal{O}(n)$ for the proposed method, where $n$ is the length of the signal [25].

For the experimental data, the proposed FD method achieved a TDR of 100%, with no false negatives or false positives, shown in Table II. In comparison, the SoP approach used in the industry has a TDR of 91.8%. Moreover, the FAR is 0% for the FD filter, and 4.2% for the SoP approach, highlighting the superior performance of the proposed FD filter. The improved performance of the proposed filter on experimental data is due to clearer distinctions between healthy and faulty signals. Simulated data includes SDNs, harder to distinguish due to noise, whereas experimental faults are larger and easier to detect. Using the residual signal $r$ instead of the output signal $y$ leads to higher accuracy in FI because $r$ both attenuates high-frequency noise through the FD filter and amplifies small deviations in frequency, amplitude, and damping, making faults more apparent. The FD filter is briefly compared to existing machine learning methods, of which the results are shown in [26].

### C. FI Results

To evaluate the overall performance of the FI filter, the harmonic mean average (HMA) is calculated. HMA is a standard metric used to assess the overall effectiveness of FI schemes [24]. The performance of the proposed hybrid model-data FI method is compared to that of a purely data-driven approach. The latter applies the FI filter directly to $y$, while the proposed method applies it to $r$, where $r$ is derived from the FD filter that incorporates model information. Additionally, the effect of training dataset size is examined by reducing it by 50% and 90%.

TABLE III

FI RESULTS (IN TERMS OF HMA) WITH DIFFERENT TRAINING SIZES FOR THE SIMULATED DATA

| Training size | Signal used | LR | KNN |
|---|---|---|---|
| 2025 | $r$ | 81.3% | 80.0% |
| | $y$ | 73.1% | 74.1% |
| 1013 | $r$ | 79.4% | 80.1% |
| | $y$ | 70.5% | 72.1% |
| 203 | $r$ | 80.1% | 78.8% |
| | $y$ | 61.4% | 66.4% |

TABLE IV

CONFUSION MATRIX OF THE PROPOSED FI FILTER RESULTS FOR THE SIMULATED DATA (SEE SECTION II FOR THE ABBREVIATIONS)

| | | FI filter | | | | | |
|---|---|---|---|---|---|---|---|
| | | EC | BN | PBN | SDN | IDN | DDN |
| Ground truth | EC | 225 | 0 | 0 | 0 | 0 | 0 |
| | BN | 0 | 225 | 0 | 0 | 0 | 0 |
| | PBN | 0 | 0 | 190 | 35 | 0 | 0 |
| | SDN | 0 | 0 | 0 | 225 | 0 | 0 |
| | IDN | 0 | 0 | 103 | 113 | 9 | 0 |
| | DDN | 0 | 0 | 0 | 0 | 1 | 224 |

TABLE V

FI RESULTS (IN TERMS OF HMA) WITH DIFFERENT TRAINING SIZES FOR THE EXPERIMENTAL DATA

| Training size | Signal used | LR | KNN |
|---|---|---|---|
| 147 | $r$ | 99.0% | 99.0% |
| | $y$ | 98.0% | 98.0% |
| 74 | $r$ | 100% | 100% |
| | $y$ | 98.0% | 98.0% |
| 15 | $r$ | 99.0% | 99.0% |
| | $y$ | 98.0% | 98.0% |

The results of the proposed FI methods using LR and KNN for the simulated data are presented in Table III. These results demonstrate that for both methods and all training sizes, applying the FI filter to the residual signal $r$ consistently outperforms applying it to the system output signal $y$, highlighting the value of model information. Among fault classes, IDNs have the lowest classification accuracy (see Table IV for the confusion matrix corresponding to the method using $r$, LR, and a training size of 2025). This is likely because their signals share similarities with those of both SDNs and partially blocked nozzles.

For comparison, the manufacturer's SoP method achieves an HMA of 45.3% on the largest training dataset. However, the SoP method has not been trained for all fault classes and would need expansion for a fair comparison.

The FI filter is also evaluated using experimental data, with results presented in Table V.

For this dataset, all methods (whether using $r$ or $y$ for FI and regardless of training set size) achieved high accuracy due to the smaller number of fault classes compared to the simulated data. The SoP method's HMA is 88.3%, but its primary

Authorized licensed use limited to: TU Delft Library. Downloaded on May 26,2026 at 12:11:59 UTC from IEEE Xplore. Restrictions apply.

$$A = \begin{bmatrix} 0 & 0 & 1 & 0 \\ 0 & 0 & 0 & 1 \\ -4.33 \times 10^{11} & -4.33 \times 10^{11} & -1.59 \times 10^{5} & 0 \\ -6.17 \times 10^{11} & -6.17 \times 10^{11} & 0 & -1.75 \times 10^{5} \end{bmatrix}$$

$$C = \begin{bmatrix} 0 & 0 & 1 & 1 \end{bmatrix}, \quad \hat{x}_a = \begin{bmatrix} 0.21 & 0.21 & 0.16 & 0.22 \end{bmatrix}^\top.$$

limitation was misclassifying IDNs as healthy. This issue does not occur with the proposed FI filter, which significantly outperforms the SoP method.

Unlike the SoP method, which performs FD and FI simultaneously using only data, the proposed method separates them and incorporates model information. Although this approach assumes prior availability of labeled faulty data, the occurrence of an unknown fault happening was briefly investigated, the results of which results are shown in [26].

## V. Conclusion

This brief has presented a method for detecting and isolating faults in the ink channels of industrial printers using model-based detection filters and LR- and KNN-based fault classifiers. Using residuals (generated for FD) in FI consistently outperformed directly using system output data, highlighting the advantages of the proposed method over purely data-driven approaches. Experimental results confirmed that the proposed FI filter outperformed the state-of-the-practice method, particularly by reducing the misclassification of faulty signals as healthy. For future work, it is recommended to experimentally evaluate the performance of the proposed methods under additional fault scenarios, such as an air bubble in the ink channel, and to investigate potential nonlinearities induced by these faults, that may have to be accounted for in the model used for FDI. Moreover, it is recommended to investigate the application of Fault Estimation, which estimates the degree of a certain fault, to the use-case.

## Appendix

The system identification results are given as $A$ and $C$, shown at the top of the page.

## Acknowledgment

The authors would like to thank Canon Production Printing Netherlands B.V. for enabling research underlying this brief. Canon Production Printing B.V. is not responsible for the accuracy of the data or the conclusion, which are solely those of the authors.

## References

[1] J. Chen and R. J. Patton, *Robust Model-Based Fault Diagnosis for Dynamic Systems*, vol. 3. Cham, Switzerland: Springer, 2012.

[2] S. X. Ding, *Model-Based Fault Diagnosis Techniques: Design Schemes, Algorithms, and Tools*. Cham, Switzerland: Springer, 2008.

[3] *Industrial Printer Manufacturer, Canon Production Printing Webpage*. Accessed: Nov. 2023. [Online]. Available: https://cpp.canon

[4] D. Lohse, "Fundamental fluid dynamics challenges in inkjet printing," *Annu. Rev. Fluid Mech.*, vol. 54, no. 1, pp. 349–382, Jan. 2022.

[5] H. Reinten et al., "Resonance behavior of a compliant piezo-driven inkjet channel with an entrained microbubble," *J. Acoust. Soc. Amer.*, vol. 151, no. 4, pp. 2545–2557, Apr. 2022.

[6] Canon Colorado M-series. (Nov. 2023). *Canon Production Printing Webpage*. [Online]. Available: https://www.canon-europe.com/business/products/wide-format-printers/colorado-m-series/

[7] U Vgel. (Nov. 2023). *Canon Production Printing Webpage*. [Online]. Available: https://cpp.canon/products/uvgel/

[8] J. M. M. Simons and M. A. Groninger, *Printing apparatus with measuring circuit for diagnosis of condition of each electromechanical transducer*, U.S. Patent 6 682 162 B2, Jan. 27, 2004.

[9] B. H. Kim, N. R. Park, and H. H. Shin, *Error detection apparatus of inkjet printer head and error detection method thereof*, U.S. Patent 8 894 178 B2, Nov. 25, 2014.

[10] M. Mihailovic et al., *Method for detecting an operating status of an inkjet nozzle*, U.S. Patent 10 144 215 B2, Dec. 4, 2018.

[11] P. Mohajerin Esfahani and J. Lygeros, "A tractable fault detection and isolation approach for nonlinear systems with probabilistic performance," *IEEE Trans. Autom. Control*, vol. 61, no. 3, pp. 633–647, Mar. 2016.

[12] E. Frisk and M. Nyberg, "Residual generation for fault diagnosis of systems described by general linear differential-algebraic equations," *IFAC Proc. Volumes*, vol. 35, no. 1, pp. 137–142, 2002.

[13] J. Dong, K. Pan, S. Pequito, and P. Mohajerin Esfahani, "Robust multivariate detection and estimation with fault frequency content information," 2023, *arXiv:2310.04922*.

[14] H. Ghasemzadeh and R. Jafari, "Physical movement monitoring using body sensor networks: A phonological approach to construct spatial decision trees," *IEEE Trans. Ind. Informat.*, vol. 7, no. 1, pp. 66–77, Feb. 2011.

[15] P. J. B. Hacking, "Classification of jetting behavior based on self-sensing piezo actuators," M.S. thesis, Dept. Mech. Eng., TU Eindhoven, The Netherlands, 2019.

[16] C. van der Ploeg, M. Alirezaei, N. van de Wouw, and P. Mohajerin Esfahani, "Multiple faults estimation in dynamical systems: Tractable design and performance bounds," *IEEE Trans. Autom. Control*, vol. 67, no. 9, pp. 4916–4923, Sep. 2022.

[17] Y. Cheng, R. Wang, and M. Xu, "A combined model-based and intelligent method for small fault detection and isolation of actuators," *IEEE Trans. Ind. Electron.*, vol. 63, no. 4, pp. 2403–2413, Apr. 2016.

[18] F. Ghanipoor, C. Murguia, P. Mohajerin Esfahani, and N. van de Wouw, "Robust fault estimators for nonlinear systems: An ultra-local model design," *Automatica*, vol. 171, Jan. 2025, Art. no. 111920.

[19] K.-S. Kwon and W. Kim, "A waveform design method for high-speed inkjet printing based on self-sensing measurement," *Sens. Actuators A, Phys.*, vol. 140, no. 1, pp. 75–83, Oct. 2007.

[20] (2024). *A Grey-Box System Identification Algorithm Provided by MATLAB*. [Online]. Available: https://nl.mathworks.com/help/ident/ref/greyest.html

[21] S. Boyd and L. Vandenberghe, *Convex Optimization*. Cambridge, U.K.: Cambridge Univ. Press, Mar. 2004.

[22] T. Fawcett, "An introduction to ROC analysis," *Pattern Recognit. Lett.*, vol. 27, no. 8, pp. 861–874, Jun. 2006.

[23] T. Cover and P. Hart, "Nearest neighbor pattern classification," *IEEE Trans. Inf. Theory*, vol. IT-13, no. 1, pp. 21–27, 1967.

[24] T. A. J. van Esch, "Hybrid model-based and data-based fault detection, isolation, and estimation for wafer handler robots," M.S. thesis, Dept. Mech. Eng., TU Eindhoven, The Netherlands, Nov. 2022.

[25] C. Albert, "A mechanistic dynamic emulator," *Nonlinear Anal., Real World Appl.*, vol. 13, no. 6, pp. 2747–2754, Dec. 2012.

[26] C. van Peijpe, F. Ghanipoor, Y. de Loore, P. Hacking, N. van de Wouw, and P. Mohajerin Esfahani, "Fault isolation for the ink deposition process in high-end industrial printers," 2024, *arXiv:2412.07545*.

Authorized licensed use limited to: TU Delft Library. Downloaded on May 26,2026 at 12:11:59 UTC from IEEE Xplore. Restrictions apply.